NJC

ROYAL SOCIETY OF CHEMISTRY

PAPER

View Article Online
View Journal | View Issue

Cite this: *New J. Chem.*, 2025, **49**, 17515

Exploring the electronic structure of unsymmetrical squaraine dyes through synthesis and functionalization

Diego dos Santos Pisoni, Marcelli Leticia da Cruz Zanirati, Luis Henrique Lapazin, Bruno Bercini de Araújo, Fabiano Severo Rodembusch, Leandra Franciscato Campo* and Felipe Lange Coelho *

Received 27th May 2025,
Accepted 2nd September 2025

DOI: 10.1039/d5nj02226f

rsc.li/njc

In this study, we report the synthesis of four unsymmetrical squaraines and their dicyanomethylene derivatives, incorporating hydroxyalkyl chains. Their electronic properties were systematically investigated in $CHCl_3$, EtOH and DMSO solutions using UV-Vis absorption and steady-state fluorescence spectroscopy. The dyes exhibit narrow absorption bands (631–689 nm), nonlinear solvent-dependent behavior, and a pronounced tendency to aggregate, as evidenced by blue-shifted absorption bands even at dilute concentrations. Introduction of a chalcogen atom induces a modest bathochromic shift of up to 14 nm, whereas substitution with dicyanomethylene groups produces a more pronounced shift of approximately 40 nm. In the excited state, these squaraines exhibit small Stokes shifts and solvent-dependent fluorescence quantum yields (0.02 to 0.2), consistent with their ground-state electronic behavior across different structural modifications. By combining experimental measurements with computational analyses, we provided a comprehensive understanding of the structural and electronic factors governing their photophysical properties. Importantly, we demonstrate that this series of unsymmetrical squaraines bearing hydroxyalkyl substituents can be further functionalized without compromising their intrinsic electronic and optical characteristics.

Introduction

Among near-infrared dyes, several classes of compounds are well established, including cyanines, phthalocyanines, porphyrins, fluorenes, BODIPY, and squaraines. Squaraine dyes, in particular, stand out not only for their distinctive photophysical and electrochemical properties but also for their remarkable stability and low cost and the broad variety of analogs that can be synthesized and further functionalized.[1–4] They are derived from an electron-deficient, unsaturated, four-membered "square" ring that bridges electron-rich subunits.[5–7] This core framework gives rise to a rigid donor–acceptor–donor (D–A–D) system with resonance-stabilized zwitterionic character, which imparts both high stability and desirable electronic features, including narrow absorption/emission bands across a wide spectral range, large molar extinction coefficients, and efficient emission.[1,8]

From a synthetic perspective, squaraines are commonly accessed through condensation of squaric acid derivatives with nitrogen-containing quaternary heterocycles as electron-rich subunits. This approach is highly versatile, enabling the incorporation of diverse substituents into both the alkyl chains and the aromatic core.[9] Moreover, core-substituted squaraines, in which an oxygen atom of the central square ring is replaced by a group such as dicyanomethylene, provide additional opportunities to modulate molecular geometry, crystallinity, and electronic properties.[10] Further functionalization, for example, through conjugation with biomolecules or other functional units, broadens their scope even more.[11–13] Owing to this exceptional tunability, squaraines have found applications across a wide range of fields, with particular emphasis on biomedicine (Fig. 1).[14–19]

In this context, the synthesis of new squaraine derivatives and the detailed study of their electronic properties remain highly relevant. Herein, we report the design and preparation of a series of unsymmetrical squaraine dyes and their dicyanomethylene derivatives, conceived as versatile synthetic building blocks. We conducted a comparative photophysical and electronic study between the parent squaraines and their derivatized counterparts, revealing how structural modifications can be introduced without compromising their intrinsic optical and electronic characteristics. These results provide valuable insights into the relationship between molecular design and the electronic structure in squaraine systems.

Instituto de Química, Universidade Federal do Rio Grande do Sul, Porto Alegre, 91501-970, Brazil. E-mail: langecoelho@ufrgs.br, campo@iq.ufrgs.br

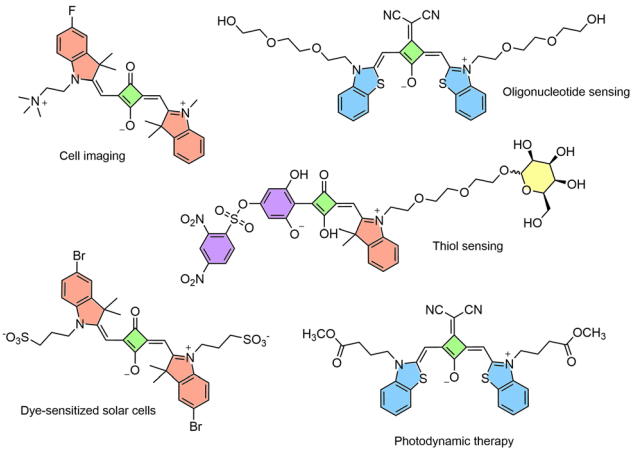

Fig. 1 Chemical structure of different functionalized squaraine dyes and their applications.

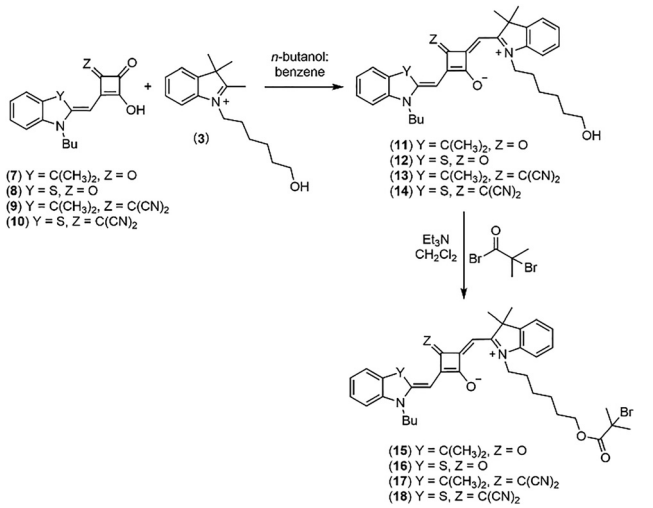

Scheme 2 Linear synthesis of unsymmetrical squaraine dyes and their derivatization.

Results and discussion

Synthesis

The unsymmetrical squaraine dyes and their dicyanomethylene-substituted derivatives were synthesized in a linear sequence, beginning with the preparation of semisquaric acid derivatives, followed by condensation with quaternary heterocyclic methylene bases, as shown in Schemes 1 and 2. One of these quaternary methylene bases was specifically designed to incorporate hydroxyalkyl chains, thereby introducing a hydroxyl group into the asymmetric squaraine at a position that does not interfere with the intrinsic electronic properties of the fluorophore.

The quaternary methylene bases were synthesized by quaternization of the corresponding heterocyclic methylene precursors, 2,3,3-trimethylindolenine or 2-methylbenzothiazole, with suitable alkylating agents such as 1-iodobutane or 6-bromo-1-hexanol. Compounds *N*-butyl-2,3,3-trimethyl-indoleninium iodide (**1**) and *N*-butyl-2-methyl-benzothiazolium iodide (**2**) were obtained by heating the respective heterocycles with an excess of 1-iodobutane (5.0 equiv.) at 145 °C under solvent-free conditions.

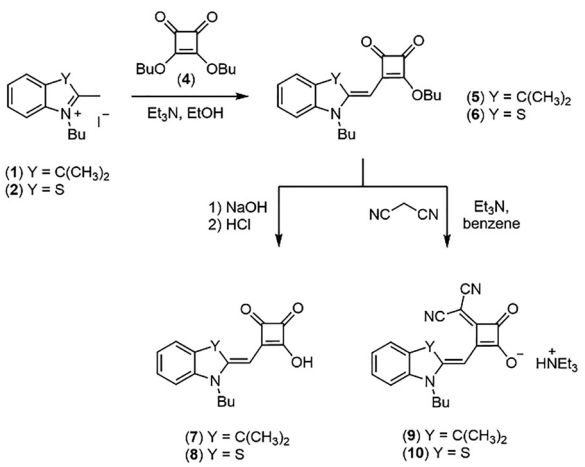

Scheme 1 Linear synthesis of semisquaric acid derivatives.

While most literature procedures describe this transformation under reflux in organic solvents, commonly acetonitrile, over several hours,[20,21] our solvent-free method significantly reduced the reaction time to just a few hours. In contrast, the preparation of *N*-(6-hydroxyhexyl)-2,3,3-trimethyl-indoleninium bromide (**3**) required the use of a solvent to proceed efficiently.

The semisquaric acid derivatives were prepared using a two-step process. First, quaternary methylene bases **1** or **2** reacted with squaric acid dibutyl ester **4** in ethanol in the presence of a stoichiometric amount of triethylamine to yield intermediates **5** and **6**. Hydrolysis of these intermediates with NaOH, followed by protonation with hydrochloric acid, yielded semisquaric acids **7** and **8**. In parallel, intermediates **5** and **6** were condensed with malononitrile in the presence of triethylamine to obtain the dicyanomethylene-functionalized semisquaric acids **9** and **10**.

Finally, semisquaric acid derivatives **7–10** were condensed with quaternary methylene base **3** under azeotropic conditions in a mixture of *n*-butanol and benzene, affording the unsymmetrical squaraines **11–14**, each bearing a hydroxyalkyl chain (Scheme 2).

The unsymmetrical nature of these squaraines was confirmed by the splitting of the vinylic proton signals in their ^{1}H NMR spectra. While symmetric squaraines typically show both vinylic protons as a single signal, unsymmetrical analogues display two distinct signals (5.96 and 5.94 ppm for **11**, 6.01 and 5.83 ppm for **12**, 6.53 and 6.47 ppm for **13**, and 6.45 and 6.19 ppm for **14**). To evaluate whether hydroxy functionalization affects the photophysical and electronic features of the squaraine core, compounds **11–14** were further derivatized with an ATRP initiator group (α-bromo ester). This transformation was carried out by stirring the squaraines in dry dichloromethane with a slight excess of 2-bromoisobutyryl bromide in the presence of triethylamine, affording derivatives **15–18**.

Photophysical characterization

The ground- and excited-state photophysical properties in solution of unsymmetrical squaraines **11–18** were investigated

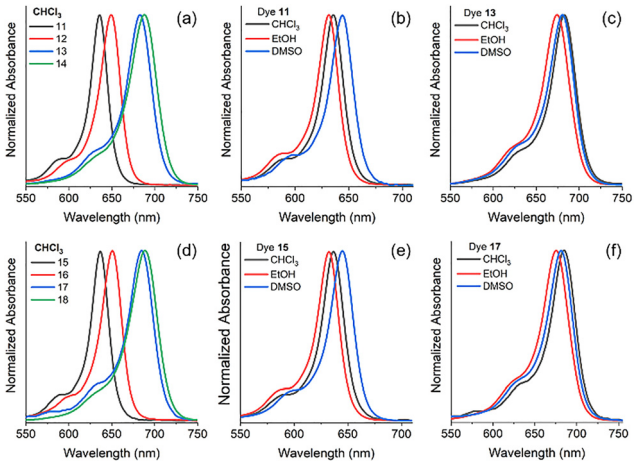

Fig. 2 Normalized UV-Vis absorption spectra for the solution of squaraines (a) **11–14** and (d) **15–18** in chloroform and squaraines (b) **11**, (c) **13**, (e) **15**, and (f) **17** in different organic solvents ($\sim 10^{-6}$ mol L^{-1}).

in chloroform, ethanol, and dimethyl sulfoxide. Representative results for the selected compounds are shown in Fig. 2. The relevant photophysical data from UV-Vis absorption and steady-state fluorescence spectroscopy for all squaraines are summarized in Table 1. These squaraines produced blue solutions with a narrow absorption band in the 631–689 nm range, which was influenced by both solvent effects and structural modifications to the square core. Introduction of the dicyanomethylene moiety induces a redshift of approximately 40 nm in the absorption maximum (Fig. 2a and d), consistent with its strong electron-withdrawing character and the preferential *cis* configuration of the squaraine backbone.[22] With respect to solvent effects, the absorption maxima varied depending on the medium, demonstrating sensitivity to the local environment (Fig. 2b–f). However, the trend with the solvent polarity was non-linear, suggesting more complex interactions, potentially involving specific solvent–solute interactions. A pronounced tendency toward aggregation was also observed, as indicated by weak, blueshifted absorption bands near 600 nm for dyes **11–12** and **15–16** and around 630 nm for dyes **13–14** and **17–18**, even at concentrations as low as 10^{-6}–10^{-7} M. In this context, solvent polarity not only stabilizes the ground state but also favors the monomeric form in solution. Additionally, the presence of sulfur atoms in certain heterocyclic methylene bases induced a modest bathochromic shift in the absorption band, but only for derivatives with an unmodified squarate core. This effect, attributed to enhanced electronic delocalization by the chalcogen,[23] was absent in the dicyanomethylene-substituted analogues.

To gain deeper insight into the nature of the electronic transitions, the experimentally determined extinction coefficient (ε) was used in combination with the Strickler–Berg formalism. In this relation, the radiative rate constant (k_e^0), as well as the oscillator strength (f_e), can be estimated from absorption spectra using eqn (1) and (2),[24]

$$f_e \approx 4.3 \times 10^{-9} \int \varepsilon d\bar{\nu} \quad (1)$$

Table 1 Ground state photophysical data of squaraine dyes **11–18** where λ_{abs} is the absorption maximum (nm), ε is the molar absorptivity ε ($\times 10^5$ M^{-1} cm^{-1}), f_e is the calculated oscillator strength, k_e^0 is the calculated radiative rate constant (10^8 s^{-1}) and τ^0 is the calculated pure radiative lifetime (ns)

Dye	Solvent	λ_{abs}	ε	f_e	k_e^0	τ^0
11	$CHCl_3$	636	2.65	0.676	1.67	5.99
	EtOH	631	2.99	0.840	2.11	4.74
	DMSO	643	3.21	0.903	2.18	4.58
12	$CHCl_3$	649	1.98	0.543	1.29	7.76
	EtOH	640	2.49	0.760	1.86	5.39
	DMSO	654	2.37	0.778	1.82	5.50
13	$CHCl_3$	683	1.85	0.587	1.26	7.94
	EtOH	674	2.10	0.650	1.43	6.99
	DMSO	680	2.30	0.697	1.51	6.63
14	$CHCl_3$	686	1.84	0.506	1.07	9.30
	EtOH	675	1.35	0.466	1.02	9.79
	DMSO	680	1.44	0.585	1.27	7.90
15	$CHCl_3$	636	2.16	1.253	3.10	3.23
	EtOH	632	2.70	0.699	1.75	5.71
	DMSO	644	3.22	0.577	1.39	7.19
16	$CHCl_3$	650	1.56	1.183	2.80	3.57
	EtOH	640	2.47	0.573	1.40	7.15
	DMSO	656	1.81	0.844	1.96	5.10
17	$CHCl_3$	686	1.53	0.547	1.16	8.60
	EtOH	676	3.67	0.744	1.63	6.14
	DMSO	682	2.24	0.472	1.01	9.86
18	$CHCl_3$	689	1.89	0.755	1.59	6.29
	EtOH	675	0.88	0.669	1.47	6.81
	DMSO	680	1.23	0.523	1.13	8.85

$$\frac{1}{\tau^0} = k_e^0 \approx 2.88 \times 10^{-9} \bar{\nu}_0^2 \int \varepsilon d\bar{\nu} \quad (2)$$

where ν_0 is the absorption maxima (in cm^{-1}) and the integral represents the area under the absorption band, plotted as molar absorptivity ε (M^{-1} cm^{-1}) *versus* wavenumber ν (cm^{-1}) for a single-electron transition.

The unsymmetrical squaraines displayed molar absorptivity coefficients on the order of 10^5 $cm^{-1}{\cdot}M^{-1}$ and a radiative rate constant of approximately 10^8 s^{-1}, irrespective of whether structural modifications were introduced at the squaric acid core or at the heterocyclic methylene substituents. The values of f_e and k_e^0 are consistent with spin- and symmetry-allowed electronic transitions, likely associated with $^1\pi \rightarrow \pi^*$ transitions. Moreover, the nearly constant radiative lifetime (τ^0) suggests that, following light absorption, these compounds populate the same excited state.

The photophysical properties of the unsymmetrical squaraines in their excited state were investigated by exciting the compounds at their respective absorption maxima (Table 2). When excited at the two distinct absorption bands observed in their UV-Vis spectra, corresponding to the monomer and aggregate forms, the resulting emission profiles were similar.

As illustrated in Fig. 3, all squaraine derivatives display fluorescence emission bands in the red region. Overall, the squaraines exhibited a small Stokes shift, which is expected in rigid molecular frameworks. Their excited-state behavior, influenced by the solvent environment and structural modifications, closely mirrors their ground-state behavior. A non-linear dependence

Table 2 Excited state photophysical data of squaraines dyes **11–18**, where λ_{em} is the emission maximum (nm), $\Delta\lambda_{ST}$ is the Stokes shift (nm/cm^{-1}) and Φ_{fl} is the fluorescence quantum yield

Dye	Solvent	λ_{em}	$\Delta\lambda_{ST}$	Φ_{fl}
11	$CHCl_3$	648	12/291	0.11
	EtOH	645	14/344	0.06
	DMSO	654	11/262	0.06
12	$CHCl_3$	663	14/325	0.20
	EtOH	656	16/381	0.06
	DMSO	672	18/410	0.07
13	$CHCl_3$	700	17/356	0.06
	EtOH	693	19/407	0.05
	DMSO	700	20/420	0.02
14	$CHCl_3$	707	21/433	0.05
	EtOH	694	19/406	0.04
	DMSO	703	23/481	0.03
15	$CHCl_3$	645	9/219	0.15
	EtOH	644	12/295	0.06
	DMSO	659	15/353	0.07
16	$CHCl_3$	661	11/256	0.19
	EtOH	655	15/358	0.06
	DMSO	671	15/341	0.07
17	$CHCl_3$	697	11/230	0.10
	EtOH	696	20/542	0.05
	DMSO	698	16/336	0.03
18	$CHCl_3$	707	18/370	0.07
	EtOH	694	19/406	0.04
	DMSO	702	22/461	0.03

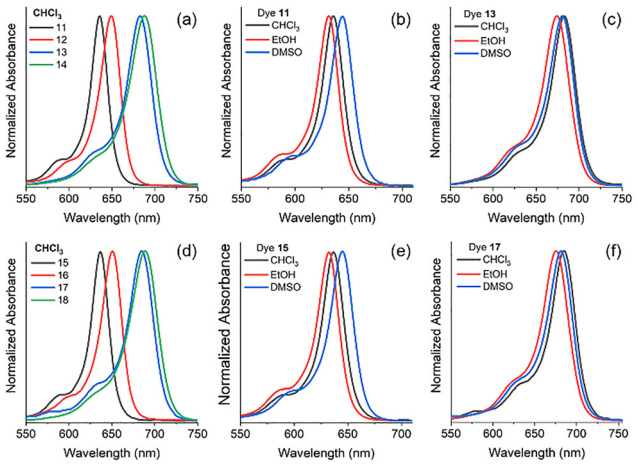

Fig. 3 Steady-state fluorescence emission spectra in solution of squaraines (a) **11–14** and (d) **15–18** in chloroform and squaraines (b) **11**, (c) **13**, (e) **15**, and (f) **17** in different organic solvents (~10^{-6} mol L^{-1}).

on solvent polarity was observed, along with a slight bathochromic shift for the benzothiazole-containing derivatives.

Similarly, incorporation of the dicyanomethylene moiety into the squarate core induced a pronounced bathochromic shift and an increase in the Stokes shift. Furthermore, the squaraines showed fluorescence quantum yields that were 2- to 3-fold higher in chloroform. Notably, despite the enhanced Stokes shift in the dicyanomethylene derivatives, no corresponding increase in quantum yield was observed, most likely due to re-absorption effects, a well-documented limitation of squaraine systems.[10,25] It is also noteworthy that both classes of derivatives, those bearing hydroxyalkyl chains (**11–14**) and those functionalized with α-bromo ester moieties (**15–18**), exhibited very similar ground- and excited-state properties. This finding highlights that further derivatization of compounds **11–14** can be carried out without compromising their intrinsic photophysical characteristics.

Theoretical calculations

The optimized geometries of compounds **15–18** (Fig. 4a) revealed planar structures that were preserved across all solvents. This planarity was expected, as it facilitates extensive π-electron delocalization, thereby stabilizing the conjugated system. In the excited state, no significant geometric changes were observed, consistent with the intrinsic rigidity of these squaraines. Symmetry analysis indicated that compounds **15** and **17** adopt C_{2h} and C_{2v} symmetry, respectively, while **16** and **18** exhibit C_1 symmetry. The molecular electrostatic potential (MEP) surfaces (Fig. 4b) further highlighted the role of functional groups in tuning electronic properties: regions of attractive potential (red) were mainly localized around polar substituents, such as oxygen atoms and cyano groups. As expected, the electrostatic potential distribution in the symmetric systems (**15** and **17**) was itself symmetric. In contrast, compounds **16** and **18** showed a slightly more pronounced repulsive potential in the benzothiazole moiety, pointing to reduced electron density in this region.

The photophysical properties of compounds **15–18** were found to be analogous, with the $S_0 \rightarrow S_1$ transition being the most probable and exhibiting high oscillator strength values. The theoretical absorption wavelengths (Table 3) were consistently blue-shifted relative to the experimental values, showing

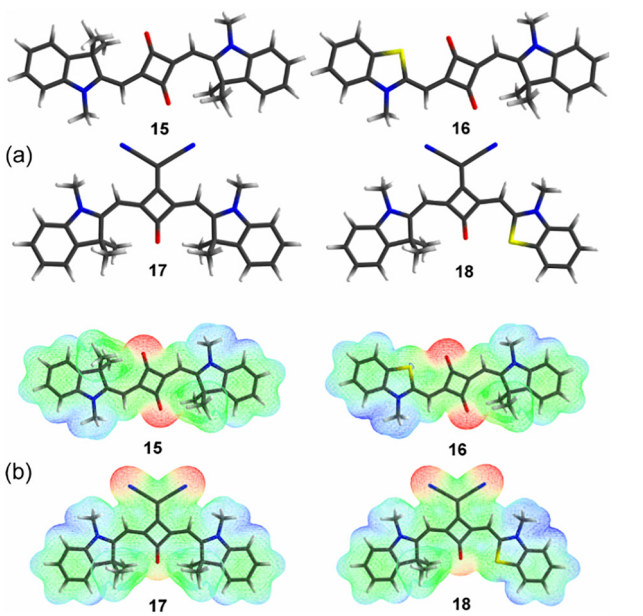

Fig. 4 (a) Optimized molecular structures of compounds **15–18** at the CAM-B3LYP(GD3BJ)/DEF2-SVP level of theory in chloroform. (b) Electrostatic potential maps of the same compounds at the CAM-B3LYP(GD3BJ)/DEF2-SVPD level of theory in chloroform, where red and blue denote regions of attractive and repulsive potential, respectively.

Table 3 Calculated photophysical properties of compounds **15–18** obtained at the CAM-B3LYP(GD3BJ)/DEF2-SVPD level of theory, where the absorption (λ_{abs}) and emission (λ_{em}) wavelengths are presented in nm, f_e is the oscillator strength of the $S_0 \rightarrow S_1$ transition and $\Delta\lambda_{ST}$ is the calculated Stokes shift (nm)

Dye	Solvent	λ_{abs}	f_e	λ_{em}	$\Delta\lambda_{ST}$
15	$CHCl_3$	558 (78)	1.789	584 (61)	26
	EtOH	543 (89)	1.853	566 (78)	23
	DMSO	556 (88)	1.800	582 (77)	26
16	$CHCl_3$	577 (73)	1.710	604 (57)	27
	EtOH	558 (82)	1.774	583 (72)	25
	DMSO	573 (83)	1.716	601 (70)	28
17	$CHCl_3$	588 (98)	1.377	617 (80)	29
	EtOH	569 (107)	1.430	596 (100)	27
	DMSO	573 (109)	1.444	602 (96)	29
18	$CHCl_3$	601 (88)	1.289	630 (77)	29
	EtOH	580 (95)	1.337	609 (85)	29
	DMSO	584 (96)	1.346	615 (87)	31

deviations ranging from 109 to 73 nm, substantially larger than the typical error margin expected for TDDFT calculations. To exclude the possibility that this discrepancy arose from the use of the CAM-B3LYP functional, additional functionals, including ωB97XD, B3LYP, M06-2X, and PBE1PBE, were evaluated. Quartarolo *et al.* demonstrated in a comprehensive study on squaraines that large deviations are common and largely independent of both the functional and the basis set.[26]

Subsequent investigations have confirmed this limitation of TDDFT and highlighted the inherent difficulties in accurately modelling squaraines, even with more computationally demanding methodologies such as multireference calculations.[27,28]

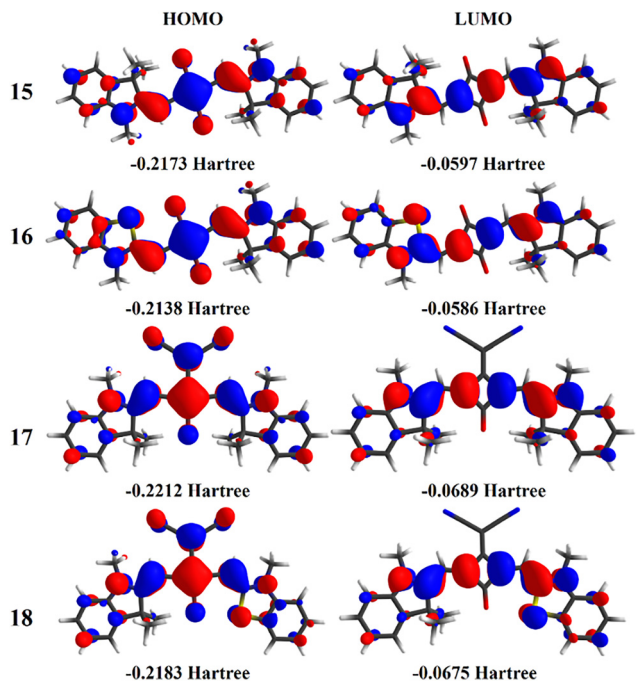

Fig. 5 HOMO and LUMO of **15–18** at the CAM-B3LYP(GD3BJ)/DEF2-SVPD level of theory in chloroform. Both orbitals were involved in the $S_0 \rightarrow S_1$ transition and had π character, making this transition a ππ* transition.

We speculate that these challenges arise not only from the intrinsic complexity of the ground and excited states, as highlighted in previous studies on one- and two-photon absorption of symmetric squaraines,[28] but also from possible self-aggregation effects, which could play a significant role in their electronic response. Fortunately, despite the quantitative discrepancies, TDDFT calculations qualitatively reproduced the experimental trends.[26,29] Overall, the absorption wavelengths in chloroform and dimethyl sulfoxide were comparable, with only a slight hypsochromic shift observed in ethanol, suggesting that the $S_0 \rightarrow S_1$ transition is relatively insensitive to the dielectric constant of solvent.

All observed transitions involved only the HOMO and the LUMO (Fig. 5), both of which are highly delocalized over the molecular framework and exhibit pronounced π-character. As charge transfer was not expected, DCT analyses were performed to evaluate the spatial separation of electron-donating and electron-accepting regions upon excitation, confirming that the $S_0 \rightarrow S_1$ transition corresponds to a local excitation (see the SI). In addition, the low Stokes shift values, consistent with the intrinsic rigidity of these conjugate systems, highlight their limited capacity to dissipate energy *via* structural reorganization.

Conclusions

This study presents a robust synthetic approach for generating unsymmetrical squaraines and their dicyanomethylene derivatives, presenting a hydroxyalkyl chain that has been functionalized with the ester group without compromising the optical properties. These dyes exhibit narrow absorption bands (631–689 nm), nonlinear solvent-sensitive behavior, and a marked tendency to aggregate, evidenced by blue-shifted absorption peaks even in dilute solutions. Furthermore, the presence of a chalcogen atom induces a modest redshift in the absorption spectrum, whereas dicyanomethylene groups trigger a more pronounced redshift. In the excited state, the squaraines display small Stokes shifts and solvent-dependent quantum yields, reflecting behavior closely mirroring their ground-state characteristics across various structural modifications. Finally, the α-bromo ester-functionalized compounds (**15–18**) show photophysical properties nearly identical to their hydroxyalkyl chain counterparts (**11–14**), which is an indicative that additional derivatization could be performed without adversely affecting their optical properties.

Experimental

Materials and methods

The reagents were purchased from commercial suppliers and used as received. Column chromatography was carried out on a silica gel 60 (70–230 mesh), and analytical thin-layer chromatography (TLC) employed aluminum plates coated with 0.2 mm silica gel 60F-254. ^1H and ^{13}C NMR data were acquired in $CDCl_3$ using a spectrometer operating at 299.98 MHz for ^1H and at

75.42 MHz for ^{13}C. Chemical shifts (δ) were reported in parts per million (ppm) relative to tetramethylsilane as an internal standard. The following abbreviations denote splitting patterns: s (singlet), d (doublet), t (triplet), q (quartet), m (multiplet), and br t (broad triplet). All observed signals were consistent with the proposed structures. IR spectra were obtained on an FTIR-ATR instrument. High-resolution mass spectrometry (HRMS) with electrospray ionization (ESI) in positive mode was performed on a Micromass Q-Tof instrument. Samples were infused at a flow rate of 5 to 10 μL min^{-1} using a 100 μL syringe. Typical operating conditions were as follows: a capillary voltage of 3.0 kV, a sample cone voltage of 33 V, an extraction cone voltage of 2.5 V, and a desolvation gas temperature of 100 °C. Nitrogen was used as the desolvation gas, and methanol served as the solvent for all samples. The UV-Vis absorption spectra were recorded on a UV spectrophotometer model Shimadzu UVPC 2450. Steady-state fluorescence emission spectra were acquired on a spectrofluorophotometer model Shimadzu RF 5300, followed by correction for the instrument's spectral sensitivity. Spectroscopic-grade solvents were used in all UV-Vis and fluorescence measurements. Fluorescence quantum yields (Φ_{fl}) were determined at 25 °C using the optical dilution method (absorbance < 0.05). Zinc phthalocyanine (ZnPc) was synthesized and purified according to the literature procedures and employed as a quantum yield standard (Φ_{fl} = 0.20 in DMSO).[30,31]

Synthesis

Quaternary heterocyclic ammonium salt precursors. Method 1: A mixture of 1-iodobutane (12.0 g, 65.2 mmol) and 2,3,3-trimethylindolenine (2.1 g, 13.2 mmol) was heated at 145 °C for 3 h. After cooling, the reaction mixture was purified by column chromatography on the silica gel using CH_2Cl_2 : MeOH (90 : 10) as the eluent, yielding 2.3 g (10.6 mmol, 80% yield) of compound **1** as a red powder. For precursor **2**, a mixture of 1-iodobutane (2.7 g, 14.7 mmol) and 2-methylbenzothiazole (11.0 g, 73.5 mmol) was heated at 145 °C for 24 h. The mixture was then cooled to 25 °C and filtered, and the solid residue was washed successively with hexane (3 × 5 mL) and diethyl ether (3 × 5 mL). The solid was dried under vacuum, affording 6.38 g (30.9 mmol, 42% yield) of compound **2** as a grey powder.

N-Butyl-2,3,3-trimethyl-indoleninium iodide (**1**). ^{1}H NMR (300 MHz, $CDCl_3$): δ (ppm) 7.80–7.69 (m, 1H), 7.68–7.52 (m, 3H), 4.67 (t, 2H, J = 7.2 Hz), 3.13 (s, 3H), 2.04–1.88 (m, 2H), 1.67 (s, 6H), 1.60–1.44 (m, 2H), 1.01 (t, 3H, J = 7.2 Hz). ^{13}C NMR (75 MHz, CDCl3): δ (ppm) 195.6, 141.5, 140.8, 130.1, 129.4, 123.4, 115.3, 54.6, 49.7, 29.9, 23.1, 20.1, 17.0, 13.6.

N-Butyl-2-methylbenzothiazolium iodide (**2**). ^{1}H NMR (300 MHz, $CDCl_3$): δ (ppm) 8.46 (d, 1H, J = 8.1 Hz), 8.12 (d, 1H, J = 8.4 Hz), 7.84 (t, 1H, J = 8.1 Hz), 7.72 (t, 1H, J = 7.8 Hz), 4.88 (t, 2H, J = 7.5 Hz), 3.45 (s, 3H), 2.04–1.86 (m, 2H), 1.64–1.44 (m, 2H), 1.00 (t, 3H, J = 6.9 Hz). ^{13}C NMR (75 MHz, $CDCl_3$): δ (ppm) 174.7, 140.8, 130.0, 129.0, 128.6, 125.0, 16.7, 51.2, 30.7, 20.1, 19.9, 13.7.

Method 2: a solution of 6-bromo-1-hexanol (3.41 g, 18.8 mmol) and 2,3,3-trimethylindolenine (2.5 g, 15.7 mmol) in acetonitrile (21 mL) was heated under reflux for 24 h. The solvent was then evaporated, and the resulting mixture was purified by column chromatography on the silica gel using CH_2Cl_2 : MeOH (80 : 20) as the eluent, yielding 2.94 g (11.3 mmol, 72% yield) of compound **3** as a red powder.

1-(6-Hydroxyhexyl)-2,3,3-trimethyl-indoleninium bromide (**3**). ^{1}H NMR (300 MHz, $CDCl_3$): δ (ppm) 7.73–7.65 (m, 1H), 7.55–7.43 (m, 3H), 4.57 (t, 2H, J = 7.8 Hz), 3.43 (t, 2H, J = 6.0 Hz), 2.99 (s, 3H), 1.94–1.78 (m, 2H), 1.52 (s, 6H), 1.48–1.27 (m, 6H). ^{13}C NMR (75 MHz, $CDCl_3$): δ (ppm) 195.4, 141.5, 140.8, 130.0, 129.5, 123.3, 115.5, 61.3, 54.5, 49.1, 31.9, 27.9, 26.1, 25.1, 23.0, 16.0.

Mono-squarate intermediate. A mixture of squaric acid (1.0 g, 8.77 mmol) and *n*-butanol (30 mL) was heated at 155 °C for 24 h using a Dean–Stark apparatus. After the solvent was removed under reduced pressure, the residue was purified by column chromatography on the silica gel, employing hexane:ethyl acetate (80 : 20) as the eluent. This procedure afforded 1.84 g (8.07 mmol, 92% yield) of 3,4-dibutoxycyclobut-3-ene-1,2-dione (**4**).

3,4-Dibutoxycyclobut-3-ene-1,2-dione (**4**). ^{1}H NMR (300 MHz, $CDCl_3$): δ (ppm) 4.69 (t, 4H, J = 6.6 Hz), 1.95–1.70 (m, 4H), 1.58–1.32 (m, 4H), 0.98 (t, 6H, J = 7.2 Hz). ^{13}C NMR (75 MHz, $CDCl_3$): δ (ppm) 189.5, 184.4, 74.4, 31.9, 18.6, 13.7.

*General procedure for the synthesis of mono-squarates **5** and **6**.* A mixture of the corresponding quaternary heterocyclic ammonium salt (1.1 equiv.), dibutyl squarate **4** (1.0 equiv.), and triethylamine (1.1 equiv.) was dissolved in ethanol and then refluxed for 30 min. The solvent was subsequently removed, and the crude product was purified by column chromatography using the n-hexane and ethyl acetate (50 : 50) mixture as the eluent.

3-Butoxy-4-[(1-butyl-3,3-dimethylindolin-2-ylidene)methyl]-3-cyclobutene-1,2-dione (**5**). Yield: 68%. FTIR (KBr, cm^{-1}): 3476, 3415, 2958, 2931, 2887, 1770, 1704, 1536, 1459, 1421, 1311, 1199. ^{1}H NMR (300 MHz, $CDCl_3$): δ (ppm) 7.32–7.23 (m, 2H), 7.07 (dt, 1H, J = 7.8 Hz and J = 0.9 Hz), 6.89 (dd, 1H, J = 7.8 Hz and J = 0.9 Hz), 5.42 (s, 1H), 4.86 (t, 2H, J = 6.6 Hz), 3.83 (t, 2H, J = 7.5 Hz), 1.92–1.81 (m, 2H), 1.80–1.69 (m, 2H), 1.62 (s, 6H), 1.59–1.38 (m, 4H), 1.01 (t, 3H, J = 7.5 Hz), 1.00 (t, 3H, J = 7.5 Hz). ^{13}C NMR (75 MHz, $CDCl_3$): δ (ppm) 192.9, 187.7, 187.6, 173.7, 168.5, 142.8, 141.0, 127.9, 122.8, 122.1, 108.6, 81.4, 73.9, 48.1, 42.9, 32.3, 28.6, 27.1, 20.5, 18.9, 14.0, 13.9.

3-Butoxy-4-[(3-butylbenzothiazol-2(3H)-ylidene)methyl]-3-cyclobutene-1,2-dione (**6**). Yield: 77%. FTIR (KBr, cm^{-1}): 3475, 3417, 2956, 2929, 2867, 1764, 1702, 1544, 1504, 1471, 1419, 1347. ^{1}H NMR (300 MHz, $CDCl_3$): δ (ppm) 7.47 (dd, 1H, J = 7.8 Hz and J = 0.9 Hz), 7.35 (dt, 1H, J = 7.8 Hz and J = 0.9 Hz), 7.16 (t, 1H, J = 7.8 Hz), 7.09 (d, 1H, J = 7.8 Hz), 5.44 (s, 1H), 4.78 (t, 2H, J = 6.6 Hz), 3.99 (t, 2H, J = 7.5 Hz), 1.92–1.69 (m, 4H), 1.58–1.40 (m, 4H), 1.01 (t, 3H, J = 7.5 Hz), 1.00 (t, 3H, J = 7.5 Hz). ^{13}C NMR (75 MHz, $CDCl_3$): δ (ppm) 193.0, 185.7, 185.3, 172.7, 159.6, 141.1, 127.0, 126.7, 123.5, 121.9, 111.1, 79.0, 73.5, 45.6, 32.1, 28.8, 20.2, 18.7, 13.8, 13.7.

*General procedure for the synthesis of mono-squarates **7** and **8**.* A solution of mono-squarates **5** or **6** in ethanol was heated to

reflux, followed by the addition of a 40% NaOH solution (1.2 equiv.). The mixture was refluxed for 15 min and then cooled to 25 °C. After addition of 2 M HCl (2.4 equiv.), the mixture was concentrated, and the residue was taken up in methylene chloride. The organic layer was concentrated to afford a crude product, consisting primarily of mono-squarates **7** and **8**, which was used without further purification in the subsequent step.

*General procedure for the synthesis of mono-squarates **9** and **10**.* To a mixture of mono-squarates **5** or **6** (1.0 equiv.), malononitrile (1.1 equiv.), and ethanol, triethylamine (1.16 equiv.) was added dropwise. The mixture was stirred at 25 °C for 2 h, after which the solvent was removed under reduced pressure. The resulting crude product, consisting predominantly of mono-squarates **9** and **10**, was used without further purification in the subsequent step.

*General procedure for the synthesis of unsymmetrical squaraines **11–14**.* A mixture of the corresponding mono-squarate (1.0 equiv.) and 1-(6-hydroxyhexyl)-2,3,3-trimethyl-indoleninium bromide (**3**) (1.0 equiv.) was dissolved in a mixture (90 : 10) of *n*-butanol/benzene (12 mL $mmol^{-1}$). The mixture was then refluxed with a Dean–Stark apparatus for 24 h. After cooling to 25 °C, the solvent was removed under reduced pressure.

Squaraine dye **11**. The resulting solid was purified by column chromatography on the silica gel using ethyl acetate as the eluent. Yield: 63%. FTIR (KBr, cm^{-1}): 3479, 3412, 2956, 2926, 2858, 1726, 1600, 1494, 1452, 1278, 1190, 1074. ^{1}H NMR (300 MHz, $CDCl_3$): δ (ppm) 7.37–7.24 (m, 4H), 7.11 (t, 2H, J = 7.5 Hz), 6.97 (d, 2H, J = 7.8 Hz), 5.96 (s, 1H), 5.94 (s, 1H), 3.97 (br t, 4H), 3.68 (t, 2H, J = 6.0 Hz), 1.90–1.68 (m, 4H), 1.76 (s, 6H), 1.75 (s, 6H), 1.66–1.36 (m, 8H), 0.96 (t, 3H, J = 7.2 Hz). ^{13}C NMR (75 MHz, $CDCl_3$): δ (ppm) 182.5, 178.9, 178.7, 170.3, 170.1, 142.5, 142.4, 142.3, 127.9, 127.8, 123.8, 122.4, 109.5, 109.4, 86.6, 62.6, 49.4, 49.3, 43.6, 43.2, 32.5, 29.2, 27.1, 26.3, 26.2, 25.0, 26.2, 25.0, 20.5, 14.0. HRMS (ESI-qTOF) m/z: $[M + H]^+$ calcd for $C_{36}H_{44}N_2O_3$ 552.3352; found 552.3359.

Squaraine dye **12**. The resulting solid was purified by column chromatography on the silica gel using ethyl acetate as the eluent. Yield: 67%. FTIR (KBr, cm^{-1}): 3469, 3414, 2954, 2926, 2856, 1577, 1494, 1450, 1425, 1259, 1078. ^{1}H NMR (300 MHz, $CDCl_3$): δ (ppm) 7.59 (dd, 1H, J = 7.8 Hz and J = 0.9 Hz), 7.41 (dt, 1H, J = 7.8 Hz and J = 1.2 Hz), 7.36–7.18 (m, 4H), 7.09 (t, 1H, J = 7.5 Hz), 6.93 (d, 1H, J = 7.8 Hz), 6.01 (s, 1H), 5.83 (s, 1H), 4.14 (t, 2H, J = 7.5 Hz), 3.93 (br t, 2H), 3.71 (t, 2H, J = 6.0 Hz), 1.85–1.72 (m, 4H), 1.76 (s, 6H), 1.75 (s, 6H), 1.68–1.40 (m, 10H), 1.00 (t, 3H, J = 7.5 Hz). ^{13}C NMR (75 MHz, $CDCl_3$): δ (ppm) 183.5, 181.5, 178.4, 174.0, 168.2, 161.4, 142.7, 142.0, 141.0, 128.0, 127.8, 127.4, 124.6, 123.0, 122.4, 122.2, 112.0, 108.9, 86.2, 86.1, 62.5, 48.8, 46.4, 42.8, 32.5, 29.6, 27.4, 26.2, 25.9. 24.8, 20.3, 13.9. HRMS (ESI-qTOF) m/z: $[M + H]^+$ calcd for $C_{33}H_{38}N_2O_3S$ 542.2603; found 542.2626.

Squaraine dye **13**. The resulting solid was purified by column chromatography on the silica gel using hexane : ethyl acetate (40 : 60) as the eluent. Yield: 70%. FTIR (KBr, cm^{-1}): 3473, 3414, 2956, 2927, 2858, 2193, 2173, 1722, 1622, 1506, 1452, 1284, 1193, 1107. ^{1}H NMR (300 MHz, $CDCl_3$): δ (ppm) 7.42–7.31 (m, 4H), 7.21 (t, 2H, J = 7.5 Hz), 7.07 (d, 2H, J = 8.1 Hz), 6.53 (s, 1H), 6.47 (s, 1H), 4.12–3.95 (m, 4H), 3.65 (t, 2H, J = 6.3 Hz), 1.93–1.70 (m, 4H), 1.78 (s, 12H), 1.68–1.40 (m, 8H), 0.99 (t, 3H, J = 7.5 Hz). ^{13}C NMR (75 MHz, $CDCl_3$): δ (ppm) 173.2, 172.1, 171.8, 167.8, 166.7, 166.5, 142.6, 142.5, 142.1, 142.0, 128.1, 124.7, 124.6, 122.4, 119.3, 119.2, 110.3, 89.2, 89.0, 62.4, 49.6, 49.5, 44.5, 44.4, 32.3, 29.5, 27.3, 26.7, 26.4, 25.5, 20.2, 14.1. HRMS (ESI-qTOF) m/z: $[M + H]^+$ calcd for $C_{39}H_{44}N_4O_2$ 600.3464; found 600.3478.

Squaraine dye **14**. The resulting solid was purified by column chromatography on the silica gel using hexane : ethyl acetate (50 : 50) as the eluent. Yield: 61%. FTIR (KBr, cm^{-1}): 3481, 3415, 2193, 2956, 2927, 2858, 2193, 2173, 1720, 1618, 1456, 1433, 1274, 1136. ^{1}H NMR (300 MHz, $CDCl_3$): δ (ppm) 7.60 (d, 1H, J = 7.8 Hz), 7.47 (t, 1H, J = 7.8 Hz), 7.37–7.23 (m, 4H), 7.12 (t, 1H, J = 7.5 Hz), 6.97 (d, 1H, J = 7.8 Hz), 6.45 (s, 1H), 6.19 (s, 1H), 4.20 (t, 2H, J = 7.2 Hz), 3.90 (t, 2H, J = 7.2 Hz), 3.63 (t, 2H, J = 6.3 Hz), 1.90–1.63 (m, 4H), 1.72 (s, 6H), 1.55–1.38 (m, 10H), 0.98 (t, 3H, J = 7.2 Hz). ^{13}C NMR (75 MHz, $CDCl_3$): δ (ppm) 173.9, 169.6, 166.3, 165.2, 163.3, 162.4, 142.3, 142.0, 140.7, 128.7, 128.1, 128.0, 125.5, 123.8, 122.6, 122.3, 119.1, 119.0, 112.7, 109.5, 88.1, 88.0, 62.3, 48.9, 47.2, 44.1, 32.3, 29.8, 27.1, 27.0, 26.4, 25.5, 20.2, 13.9. HRMS (ESI-qTOF) m/z: $[M + H]^+$ calcd for $C_{36}H_{38}N_4O_2S$ 590.2715; found 590.2710.

*General procedure for the synthesis of unsymmetrical squaraine derivatives **15–18**.* Under a nitrogen atmosphere, 2-bromo-2-methylpropionyl bromide (1.2 equiv.) was added dropwise to a stirred solution of the corresponding squaraines **11–14** (1.0 equiv.) and triethylamine (1.2 equiv.) in dichloromethane. The mixture was kept at 0 °C for 1 h under a nitrogen atmosphere and then gradually warmed to 25 °C, where it was stirred overnight. The reaction mixture was subsequently washed four times with saturated aqueous NH_4Cl (4 × 150 mL) and four times with water (4 × 150 mL). The organic phase was dried over Na_2SO_4 and filtered and the solvent was removed under reduced pressure.

Squaraine dye **15**. The resulting solid was purified by column chromatography on the silica gel using hexane : ethyl acetate (80 : 20) as the eluent. Yield: 88%. FTIR (KBr, cm^{-1}): 3430, 2956, 2927, 2859, 1731, 1598, 1496, 1454, 1278, 1191, 1170, 1076. ^{1}H NMR (300 MHz, $CDCl_3$): δ (ppm) 7.40–7.20 (m, 4H), 7.11 (t, 2H, J = 7.2 Hz), 6.97 (d, 1H, J = 7.8 Hz), 6.95 (d, 1H, J = 7.8 Hz), 5.95 (s, 1H), 5.93 (s, 1H), 4.14 (t, 2H, J = 6.3 Hz), 3.98 (br s, 4H), 1.90 (s, 6H), 1.82–1.60 (m, 6H), 1.76 (s, 12H), 1.55–1.37 (m, 6H), 0.96 (t, 3H, J = 7.2 Hz). ^{13}C NMR (75 MHz, $CDCl_3$): δ (ppm) 182.5, 179.6, 179.2, 171.8, 170.3, 169.9, 142.5, 142.3, 127.9, 123.8, 122.4, 109.5, 109.5, 86.7, 86.6, 65.9, 56.1, 49.3, 49.2, 43.6, 30.9, 29.8, 29.2, 28.4, 27.2, 27.1, 26.8, 25.8, 20.5, 14.0. HRMS (ESI-qTOF) m/z: $[M + H]^+$ calcd for $C_{40}H_{49}BrN_2O_4$ 700.2864; found 700.2879.

Squaraine dye **16**. The resulting solid was purified by column chromatography on the silica gel using hexane : ethyl acetate (80 : 20) as the eluent. Yield: 92%. FTIR (KBr, cm^{-1}):

3438, 2956, 2927, 2859, 1731, 1594, 1496, 1452, 1421, 1259, 1106, 1079. ^{1}H NMR (300 MHz, $CDCl_3$): δ (ppm) 7.55 (d, 1H, J = 7.8 Hz), 7.38 (t, 1H, J = 7.8 Hz), 7.33–7.14 (m, 4H), 7.05 (t, 1H, J = 7.8 Hz), 6.88 (d, 1H, J = 7.8 Hz), 5.99 (s, 1H), 5.77 (s, 1H), 4.24–4.02 (m, 4H), 3.98 (br t, 2H), 1.89 (s, 6H), 1.86–1.60 (m, 6H), 1.74 (s, 6H), 1.53–1.36 (m, 6H), 0.97 (t, 3H, J = 7.5 Hz). ^{13}C NMR (75 MHz, $CDCl_3$): δ (ppm) 181.2, 179.2, 179.1, 174.6, 171.8, 168.0, 161.5, 142.8, 142.0, 141.0, 128.9, 127.8, 127.4, 124.7, 123.0, 122.4, 122.3, 112.0, 108.8, 86.2, 66.0, 56.1, 48.8, 46.4, 43.3, 30.9, 29.6, 28.4, 27.4, 26.9, 26.8, 25.8, 20.3, 13.9. HRMS (ESI-qTOF) m/z: $[M + H]^+$ calcd for $C_{37}H_{43}BrN_2O_4S$ 690.2127; found 690.2137.

Squaraine dye **17**. The resulting solid was purified by column chromatography on the silica gel using dichloromethane:ethyl acetate (95 : 5) as the eluent. Yield: 86%. FTIR (KBr, cm^{-1}): 3469, 2958, 2927, 2861, 2192, 2175, 1727, 1494, 1286, 1195, 1108. ^{1}H NMR (300 MHz, $CDCl_3$): δ (ppm) 7.42–7.28 (m, 4H), 7.25–7.14 (m, 2H), 7.11–7.00 (m, 2H), 6.52 (s, 1H), 6.50 (s, 1H), 4.16 (t, 2H, J = 6.6 Hz), 4.08–3.95 (m, 4H), 1.92 (s, 6H), 1.90–1.65 (m, 6H), 1.77 (s, 12H), 1.60–1.40 (m, 6H), 0.98 (t, 3H, J = 7.5 Hz). ^{13}C NMR (75 MHz, $CDCl_3$): δ (ppm) 173.2, 172.2, 171.8, 167.9, 167.0, 166.6, 142.6, 142.5, 142.1, 142.0, 128.2, 124.7, 122.5, 122.4, 119.3, 119.2, 110.3, 110.1, 89.4, 89.2, 66.0, 56.3, 49.6, 49.5, 44.4, 30.9, 29.6, 28.3, 27.3, 26.8, 26.7, 26.4, 25.8, 20.3, 14.1. HRMS (ESI-qTOF) m/z: $[M + H]^+$ calcd for $C_{43}H_{49}BrN_4O_3$ 748.2988; found 748.3019.

Squaraine dye **18**. The resulting solid was purified by column chromatography on the silica gel using dichloromethane:ethyl acetate (95 : 5) as the eluent. Yield: 83%. FTIR (KBr, cm^{-1}): 3479, 3412, 2958, 2929, 2660, 2191, 2171, 1730, 1620, 1516, 1471, 1456, 1274, 1114. ^{1}H NMR (300 MHz, $CDCl_3$): δ (ppm) 7.64 (d, 1H, J = 7.8 Hz), 7.50 (t, 1H, J = 7.8 Hz), 7.40–7.25 (m, 4H), 7.15 (t, 1H, J = 7.8 Hz), 6.99 (d, 1H, J = 7.8 Hz), 6.54 (s, 1H), 6.29 (s, 1H), 4.23 (t, 2H, J = 7.5 Hz), 4.17 (t, 2H, J = 6.6 Hz), 3.94 (t, 2H, J = 7.5 Hz), 1.93 (s, 6H), 1.92–1.75 (m, 4H), 1.80–1.65 (m, 2H), 1.75 (s, 6H), 1.62–1.41 (m, 6H), 1.01 (t, 3H, J = 7.5 Hz). ^{13}C NMR (75 MHz, $CDCl_3$): δ (ppm) 173.8, 171.7, 169.4, 166.4, 165.2, 163.2, 162.3, 142.3, 141.9, 140.7, 128.7, 127.9, 127.8, 125.4, 123.7, 122.5, 122.2, 119.1, 118.8, 112.6, 109.4, 88.1, 88.0, 65.9, 56.1, 48.7, 47.1, 43.9, 30.8, 29.8, 28.2, 27.1, 27.0, 26.3, 25.7, 20.2, 13.8. HRMS (ESI-qTOF) m/z: $[M + H]^+$ calcd for $C_{40}H_{43}BrN_4O_3S$ 738.2239; found 738.2225.

Theoretical calculations. The photophysical properties of compounds **15–18** were investigated using density functional theory (DFT) and time-dependent DFT (TD-DFT), as implemented in Gaussian 16 revision A03.[32] The range-separated hybrid functional CAM-B3LYP[33] was selected due to its proven reliability in predicting excited-state properties, as demonstrated in various benchmark studies.[34] The basis set was chosen to balance computational efficiency and accuracy. Geometry optimizations were performed using the double-ζ basis set DEF2-SVP, which offers reliable molecular structures at a reasonable computational cost, particularly for medium to large molecules when paired with hybrid functionals.[35] To improve the accuracy of absorption and emission wavelength predictions, diffuse functions were added to the basis set (DEF2-SVPD), enhancing the description of excited states. Furthermore, Grimme's empirical dispersion correction with Becke–Johnson damping (GD3BJ) was applied to all calculations, as it is widely recommended for standard DFT procedures.[36–38] In summary, both ground and excited-state geometries were optimized at the CAM-B3LYP(GD3BJ)/DEF2-SVP level of theory. All Cartesian coordinates are provided in the SI. To reduce computational costs, certain simplifications were applied to the molecular structures: specifically, the long alkyl chains in all systems were replaced with methyl groups, as they do not significantly contribute to the delocalized π-orbitals involved in electronic transitions. At the same level of theory, the absence of imaginary frequencies confirmed that the optimized geometries correspond to the true minimum on the potential energy surface. Absorption and emission wavelengths were calculated at the CAM-B3LYP(GD3BJ)/DEF2-SVPD level of theory, considering the first eight excited states. Solvent effects for chloroform, ethanol, and dimethyl sulfoxide were modeled implicitly using the SMD-PCM approach.[39] Additionally, charge transfer characteristics were analyzed using the DCT protocol implemented in Multiwfn 3.8.[40–42]

Author contributions

Diego dos Santos Pisoni, Marcelli Leticia da Cruz Zanirati, and Luis Henrique Lapazin: investigation. Bruno Bercini de Araujo: investigation and writing – original draft. Fabiano Severo Rodembusch: writing – original draft, writing – review and editing, resources, conceptualization, funding acquisition, supervision, and project administration. Leandra Franciscato Campo: resources, conceptualization, supervision, and writing – review and editing. Felipe Lange Coelho: conceptualization, writing – original draft, and writing – review and editing.

Conflicts of interest

There are no conflicts to declare.

Data availability

Details about the application of the Strickler–Berg relation, additional photophysical and theoretical data and copies of NMR spectra for all compounds are available in supporting information. See DOI: **https://doi.org/10.1039/d5nj02226f**.

Acknowledgements

The authors would like to acknowledge CNPq (304368/2023-7 and 402854/2023-3) and Coordenação de Aperfeiçoamento de Pessoal de Nível Superior – Brazil (CAPES) – Finance Code 001 for their financial support.

References

1 W. Qiao and Z. Li, Recent progress of squaraine-based fluorescent materials and their biomedical applications, *Symmetry*, 2022, **14**, 966.
2 S. Pascal, S. David, C. Andraud and O. Maury, Near-infrared dyes for two-photon absorption in the short-wavelength infrared: strategies towards optical power limiting, *Chem. Soc. Rev.*, 2021, **50**, 6613–6658.
3 K. Yan, Z. Hu, P. Yu, Z. He, Y. Chen, J. Chen, H. Sun, S. Wang and F. Zhang, Ultra-photostable small-molecule dyes facilitate near-infrared biophotonics, *Nat. Commun.*, 2024, **15**, 2593.
4 N. G. Medeiros, C. A. Braga, V. S. Câmara, R. C. Duarte and F. S. Rodembusch, Near-infrared fluorophores based on heptamethine cyanine dyes: From their synthesis and photophysical properties to recent optical sensing and bioimaging applications, *Asian J. Org. Chem.*, 2022, **11**, e202200095.
5 E. Terpetschnig, H. Szmacinski and J. R. Lakowicz, Synthesis, spectral properties and photostabilities of symmetrical and unsymmetrical squarines; A new class of flourophores with long-wavelength exiciation and emission, *Anal. Chim. Acta*, 1993, **282**, 633–641.
6 J. Ros-Lis, R. Martínez-Máñez, F. Sancenón, J. Soto, M. Spieles and K. Rurack, Squaraines as reporter units: Insights into their photophysics, protonation, and metal-ion coordination behaviour, *Chem. – Eur. J.*, 2008, **14**, 10101–10114.
7 K. Ilina, W. M. MacCuaig, M. Laramie, J. N. Jeouty, L. R. McNally and M. Henary, Squaraine dyes: Molecular design for different applications and remaining challenges, *Bioconjugate Chem.*, 2019, **31**, 194–213.
8 S. Khopkar and G. Shankarling, Synthesis, photophysical properties and applications of NIR absorbing unsymmetrical squaraines: A review, *Dyes Pigm.*, 2019, **170**, 107645.
9 S. Sarasiya, S. Sarasiya and M. Henary, Exploration of NIR squaraine contrast agents containing various heterocycles: Synthesis, optical properties and applications, *Pharmaceuticals*, 2023, **16**, 1299.
10 U. Mayerhöffer, M. Gsänger, M. Stolte, B. Fimmel and F. Würthner, Synthesis and molecular properties of acceptor-substituted squaraine dyes, *Chem. – Eur. J.*, 2013, **19**, 218–232.
11 Y. He, J. Mei, M. Zhou, Y. Zhang, Q. Liang, S. Xu and Z. Li, Colorimetric and fluorescent probe for highly selective and sensitive recognition of Cu^{2+} and Fe^{3+} based on asymmetric squaraine dye, *Inorg. Chem. Commun.*, 2022, **142**, 109592.
12 M. Jo, S. Choi, J. H. Jo, S. Y. Kim, P. S. Kim, C. H. Kim, H. J. Son, C. Pac and S. O. Kang, Utility of squaraine dyes for dye-sensitized photocatalysis on water or carbon dioxide reduction, *ACS Omega*, 2019, **4**, 14272–14283.
13 L. Beverina and P. Salice, Squaraine compounds: Tailored design and synthesis towards a variety of material science applications, *Eur. J. Org. Chem.*, 2010, 1207–1225.
14 V. Grande, F. Doria, M. Freccero and F. Würthner, An aggregating amphiphilic squaraine: A light-up probe that discriminates parallel G-quadruplexes, *Angew. Chem., Int. Ed.*, 2017, **56**, 7520–7524.
15 T. Fukuda, S. Yokomizo, S. Casa, H. Monaco, S. Manganiello, H. Wang, X. Lv, A. D. Ulumben, C. Yang, M. W. Kang, K. Inoue, M. Fukushi, T. Sumi, C. Wang, H. Kang, K. Bao, M. Henary, S. Kashiwagi and H. S. Choi, Fast and durable intraoperative near-infrared imaging of ovarian cancer using ultrabright squaraine fluorophores, *Angew. Chem., Int. Ed.*, 2022, **61**, e202117330.
16 Y. Wei, X. Hu, L. Shen, B. Jin, X. Liu, W. Tan and D. Shangguan, Dicyanomethylene substituted benzothiazole squaraines: The efficiency of photodynamic therapy *in vitro* and *in vivo*, *EBioMedicine*, 2017, **23**, 25–33.
17 S. A. Al-horaibi, E. M. Garoon, N. A. Bhise, S. T. Gaikwad and A. S. Rajbhoj, The effect of bis-carboxylic groups of squarylium dyes on the efficiency of dye-sensitized solar cells, *Chem. Pap.*, 2020, **74**, 1769–1778.
18 S. A. Al-horaibi, A. M. Asiri, R. M. El-Shishtawy, S. T. Gaikwad and A. S. Rajbhoj, Indoline and benzothiazole-based squaraine dye-sensitized solar cells containing bis-pendent sulfonate groups: Synthesis, characterization and solar cell performance, *J. Mol. Struct.*, 2019, **1195**, 591–597.
19 X. Li, J. Ma, Y. Huang, Z. Wang and Z. Lu, Highly sensitive squaraine-based water-soluble far-red/near-infrared chromofluorogenic thiophenol probe, *ACS Sens.*, 2017, **2**, 599–605.
20 S. Cao, L. C. da Silva and K. Landfester, Light-Activated Membrane Transport in Polymeric Cell-Mimics, *Angew. Chem., Int. Ed.*, 2022, **61**, e202205266.
21 M. Matsui, H. Mase, J. Jin, K. Funabiki, T. Yoshida and H. Minoura, Application of semisquaric acids as sensitizers for zinc oxide solar cell, *Dyes Pigm.*, 2006, **70**, 48–53.
22 C. Qin, Y. Numata, S. Zhang, X. Yang, A. Islam, K. Zhang, H. Chen and L. Han, Novel near-infrared squaraine sensitizers for stable and efficient dye-sensitized solar cells, *Adv. Funct. Mater.*, 2014, **24**, 3059–3066.
23 T. D. Martins, M. L. Pacheco, R. E. Boto, P. Almeida, J. P. S. Farinha and L. V. Reis, Fundamentals in the chemistry of cyanine dyes: A review, *Dyes Pigm.*, 2017, **147**, 120–129.
24 S. J. Strickler and R. A. Berg, Relationship between absorption intensity and fluorescence lifetime of molecules, *J. Chem. Phys.*, 1962, **37**, 814–822.
25 P. Salice, J. Arnbjerg, B. W. Pedersen, R. Toftegaard, L. Beverina, G. A. Pagani and P. R. Ogilby, Photophysics of squaraine dyes: Role of charge-transfer in singlet oxygen production and removal, *J. Phys. Chem. A*, 2010, **114**, 2518–2525.
26 A. Quartarolo, E. Sicilia and N. Russo, On the potential use of squaraine derivatives as photosensitizers in photodynamic therapy: A TDDFT and RICC2 survey, *J. Chem. Theory Comput.*, 2009, **5**, 1849–1857.
27 F. Bassal, A. D. Laurent, B. Le Guennic and D. Jacquemin, Exploring the excited-states of squaraine dyes with TD-DFT, SOS-CIS(D) and ADC(2), *Dyes Pigm.*, 2017, **138**, 169–175.
28 F. J. Avila Ferrer, C. Angeli, J. Cerezo, S. Coriani, A. Ferretti and F. Santoro, The intriguing case of the one-photon and

two-photon absorption of a prototypical symmetric squaraine: Comparison of TDDFT and wave-function methods, *ChemPhotoChem*, 2019, **3**, 778–793.

29 R. Borrelli, S. Ellena and C. Barolo, Theoretical and experimental determination of the absorption and emission spectra of a prototypical indolenine-based squaraine dye, *Phys. Chem. Chem. Phys.*, 2014, **16**, 2390–2398.

30 J. Savolainen, D. van der Linden, N. Dijkhuizen and J. L. Herek, Characterizing the functional dynamics of zinc phthalocyanine from femtoseconds to nanoseconds, *J. Photochem. Photobiol., A*, 2008, **196**, 99–105.

31 D. S. Pisoni, M. P. de Abreu, C. L. Petzhold, F. S. Rodembusch and L. F. Campo, Synthesis, photophysical study and BSA association of water-insoluble squaraine dyes, *J. Photochem. Photobiol., A*, 2013, **252**, 77–83.

32 M. J. Frisch, G. W. Trucks, H. B. Schlegel, G. E. Scuseria, M. A. Robb, J. R. Cheeseman, G. Scalmani, V. Barone, G. A. Petersson, H. Nakatsuji, X. Li, M. Caricato, A. V. Marenich, J. Bloino, B. G. Janesko, R. Gomperts, B. Mennucci, H. P. Hratchian, J. V. Ortiz, A. F. Izmaylov, J. L. Sonnenberg, D. Williams-Young, F. Ding, F. Lipparini, F. Egidi, J. Goings, B. Peng, A. Petrone, T. Henderson, D. Ranasinghe, V. G. Zakrzewski, J. Gao, N. Rega, G. Zheng, W. Liang, M. Hada, M. Ehara, K. Toyota, R. Fukuda, J. Hasegawa, M. Ishida, T. Nakajima, Y. Honda, O. Kitao, H. Nakai, T. Vreven, K. Throssell, J. A. Montgomery, Jr., J. E. Peralta, F. Ogliaro, M. J. Bearpark, J. J. Heyd, E. N. Brothers, K. N. Kudin, V. N. Staroverov, T. A. Keith, R. Kobayashi, J. Normand, K. Raghavachari, A. P. Rendell, J. C. Burant, S. S. Iyengar, J. Tomasi, M. Cossi, J. M. Millam, M. Klene, C. Adamo, R. Cammi, J. W. Ochterski, R. L. Martin, K. Morokuma, O. Farkas, J. B. Foresman and D. J. Fox, *Gaussian 16, Revision A.03*, Gaussian, Inc., Wallingford CT, 2016.

33 T. Yanai, D. P. Tew and N. C. Handy, A new hybrid exchange-correlation functional using the Coulomb-attenuating method (CAM-B3LYP), *Chem. Phys. Lett.*, 2004, **393**, 51–57.

34 R. Sarkar, M. Boggio-Pasqua, P. F. Loos and D. Jacquemin, Benchmarking TD-DFT and wave function methods for oscillator strengths and excited-state dipole moments, *J. Chem. Theory Comput.*, 2021, **17**, 1117–1132.

35 M. Bursch, J. M. Mewes, A. Hansen and S. Grimme, Best-practice DFT protocols for basic molecular computational chemistry, *Angew. Chem., Int. Ed.*, 2022, **61**, e202205735.

36 S. Grimme, J. Antony, S. Ehrlich and H. Krieg, A consistent and accurate ab initio parametrization of density functional dispersion correction (DFT-D) for the 94 elements H-Pu, *J. Chem. Phys.*, 2010, **132**, 154104.

37 S. Grimme, S. Ehrlich and L. Goerigk, Effect of the damping function in dispersion corrected density functional theory, *J. Comput. Chem.*, 2011, **32**, 1456–1465.

38 L. Goerigk and N. Mehta, A trip to the density functional theory zoo: Warnings and recommendations for the user, *Aust. J. Chem.*, 2019, **72**, 563–573.

39 A. V. Marenich, C. J. Cramer and D. G. Truhlar, Universal solvation model based on solute electron density and on a continuum model of the solvent defined by the bulk dielectric constant and atomic surface tensions, *J. Phys. Chem. B*, 2009, **113**, 6378–6396.

40 T. Le Bahers, C. Adamo and I. Ciofini, A qualitative index of spatial extent in charge-transfer excitations, *J. Chem. Theory Comput.*, 2011, **7**, 2498–2506.

41 T. Lu and F. Chen, Multiwfn: A multifunctional wavefunction analyzer, *J. Comput. Chem.*, 2012, **33**, 580–592.

42 T. Lu, A comprehensive electron wavefunction analysis toolbox for chemists, Multiwfn, *J. Chem. Phys.*, 2024, **161**, 082503.

